

# Efficient Cross-Country Data Acquisition Strategy for ADAS via Street-View Imagery

Yin Wu<sup>1,2</sup>, Daniel Slieter<sup>3</sup>, Carl Esselborn<sup>1</sup>,  
Ahmed Abouelazm<sup>4</sup>, Tsung Yuan Tseng<sup>1</sup>, and J. Marius Zöllner<sup>2,4</sup>

## Abstract—

Deploying Advanced Driver-Assistance Systems (ADAS) and Automated Driving Systems (ADS) across countries remains challenging due to differences in legislation, traffic infrastructure, and visual conventions, which introduce domain shifts that degrade perception performance. Traditional cross-country data collection relies on extensive on-road driving, making it costly and inefficient to identify representative locations. To address this, we propose a street-view-guided data acquisition strategy that leverages publicly available imagery to identify places of interest (POI). Two POI scoring methods are introduced: a KNN-based feature distance approach using a vision foundation model, and a visual-attribution approach using a vision-language model. To enable repeatable evaluation, we adopt a *collect-detect* protocol and construct a co-located dataset by pairing the Zenseact Open Dataset with Mapillary street-view images. Experiments on traffic sign detection, a task particularly sensitive to cross-country variations in sign appearance, show that our approach achieves performance comparable to random sampling while using only half of the target-domain data. We further provide cost estimations for full-country analysis, demonstrating that large-scale street-view processing remains economically feasible. These results highlight the potential of street-view-guided data acquisition for efficient and cost-effective cross-country model adaptation.

**Index Terms**—Autonomous Driving, ADAS, Domain Adaptation, Multi-Modal LLM

## I. INTRODUCTION

The deployment of ADAS and ADS in new countries remains challenging due to *domain shift*: models trained in a source market often degrade when exposed to different legislation, traffic infrastructure, and visual conventions [1]. As shown in Fig. 1, even within the European Union, traffic signs may differ across countries (e.g., yellow-background warning signs in Poland vs. white background in Germany), creating non-trivial distribution gaps that affect perception modules.

A straightforward yet costly solution is to perform large-scale test drives in each target country, which is both resource-intensive and time-consuming. Route planning by road type (e.g., urban, highway, suburban) can reduce some effort, but planning those truly informative locations into test drive before visiting there is still infeasible. To obtain *a priori* insights before driving, experts increasingly leverage global street-view imagery from platforms such as Google Maps [3] and Mapillary [4] to explore candidate locations and identify



Fig. 1: Traffic signs exhibit strong domain shifts across countries. In Poland, warning signs have yellow backgrounds, whereas in Sweden, generic warning signs use a vertical line instead of an exclamation mark [2].

Places of Interests (POIs) whose visual or semantic attributes differ from those in the source country. However, the massive amount of available imagery and its highly variable quality (resolution, blur, viewpoint, and capture device) make both manual inspection and automated POI discovery extremely challenging.

Recent advances in vision foundation models [5] and Vision Large Language Models (vLLMs) [6], [7] offer new opportunities for addressing these challenges. Such models demonstrate strong zero- and few-shot generalization and can reason about scene semantics directly from visual inputs. In this work, we first systematically propose a cross-country data acquisition strategy, which prioritizes the POI for data collection. Then, we leverage the off-the-shelf foundation models and investigate two POI scoring method: (1) a k-Nearest-Neighbor (KNN)-based feature distance method, which borrow the idea from standard Out-of-Distribution (OOD) detection [8]. (2) a vLLM-based visual attributing method that annotates traffic attributes, making POI interpretable.

While travelling to different countries and collecting data based on detected POI is logically infeasible, to enable repeatable evaluation, we adopt a *collect-detect* protocol and construct a co-located dataset by pairing the Zenseact Open Dataset (ZOD) [2] with street-view images retrieved from Mapillary [4]. We study cross-country perception adaptation with Germany as the source domain and Poland, Sweden,

<sup>1</sup>Authors are with the CARIAD SE, Germany

<sup>2</sup>Authors are with the Karlsruhe Institute of Technology, Germany

<sup>3</sup>Authors are with the Esslingen University of Applied Sciences, Germany

<sup>4</sup>Authors are with the FZI Research Center for Information Technology, Germany

and France as target domains, using traffic sign detection as the representative task due to its strong sensitivity to country legislation. Results show that while both methods outperform the random selection baseline, the vLLM-based approach is more stable and achieves comparable effectiveness using only 50% of the data required by random selection.

In summary, our contributions are:

- We introduce a street-view-guided *pre-drive* data acquisition strategy for cross-country model adaptation and propose two POI exploration methods based on vision foundation models and vLLM.
- We propose a *collect-detect* evaluation protocol and construct a co-located dataset pairing ZOD with Mapillary street-view imagery, enabling controlled and repeatable assessment.
- We conduct comprehensive experiments to demonstrate the effectiveness of our proposed methods. In particular, the vLLM-based approach achieves comparable performance while requiring only half of the target-domain data used by random selection.

## II. RELATED WORK

In this section, we first discuss Traffic Sign Detection (TSD), which serves as the model under test in our study. We then review three closely related research directions: active learning, domain adaptation, and OOD detection, and explain how they differ from our objective. Finally, we summarize recent progress in vLLM and its applications, which inspires our approach.

### A. Traffic Sign Detection and Recognition

TSD and Traffic Sign Recognition (TSR) are critical perception components in ADAS and ADS, enabling functions such as intelligent speed assistance (ISA). TSD can be formulated as a standard object detection problem, where models such as YOLO [9], Faster R-CNN [10], and RetinaNet [11] are commonly preferred over transformer-based models [12] due to their favorable accuracy-speed trade-offs. However, TSR presents unique challenges: a large number of fine-grained categories (e.g., different speed limits), highly imbalanced class distributions, and the small physical size of traffic signs within high-resolution driving scenes.

In this work, we do not aim to develop a new state-of-the-art TSR model; instead, we focus on improving cross-country domain adaptation efficiency through data selection and collection strategies. Thus we focus on a binary TSD (sign vs. background) as a representative ADAS perception task.

### B. Active Learning, Domain Adaptation, and Out-of-Distribution Detection

Prior studies have extensively discussed the challenges of domain shift and data selection.

Active learning seeks to identify the more informative samples for labeling, thereby reducing annotation costs while maintaining performance [13]. Typical approaches exploit model-internal signals, such as uncertainty-based [14] and

diversity-based [15] selection, to iteratively query unlabeled samples for annotation. Although active learning could, in principle, support our cross-country POI selection, standard settings assume that labeled and unlabeled data are drawn from the *same* underlying distribution. In contrast, our task involves two distinct resources: high-quality driving data for model training and diverse street-view imagery for POI exploration.

Domain adaptation represents another major line of research addressing domain shift between source and target domains [5], [16]–[18]. These approaches aim to align feature distributions using metrics such as maximum mean discrepancy [5], adversarial learning [16], or reconstruction-based objectives [17]. Instead of designing a model-centric alignment framework, our work adopts a *data-centric* perspective, exploring how selective data collection can improve finetuning efficiency across countries.

A third related direction is OOD detection [8], [19]–[21], which seeks to identify or reject unseen samples during inference to avoid unsafe predictions in safety-critical settings. Similar to active learning, many OOD approaches leverage model-internal uncertainty [19], [20] or feature-space distance measures [8] to detect data that deviates from the training distribution. While OOD detection and our work share the goal of handling distribution shifts, their purposes differ: rather than rejecting OOD samples, we intentionally identify and leverage them to enhance model generalization and cross-country validation coverage.

Although our problem setting does not exactly fall into any of these paradigms, it is conceptually related to all three. Inspired by foundation model-guided adaptation [21], we employ pretrained vision encoders and a KNN-based feature distance mechanism to detect informative locations, functioning as an “active learning style” method.

### C. vLLM and Visual Attribution

Recent advances in Large Language Model (LLM) and vLLM have demonstrated remarkable zero-shot generalization across diverse perception and reasoning tasks [6], [7]. Early progress in vision-language alignment can be traced back to CLIP [22], which performs contrastive learning between paired text and image representations. CLIP has shown strong generalization ability across downstream tasks and has since been widely adopted as a pretrained backbone for multimodal understanding [21], [23].

Building upon these developments, several studies have integrated LLM and vLLM into the autonomous driving pipeline. For example, Wu *et al.* [24] and Zhao *et al.* [25] explore offline scenario extraction and understanding, while Sima *et al.* [26] and Tian *et al.* [27] utilize vLLMs to simulate human-like reasoning in challenging driving situations on a real-time system. Zhong *et al.* [28] studied visual question answering targeting on small objects.

Within this context, *visual attribution* has emerged as an effective approach for interpretable image classification and pseudo-label generation [29], [30]. Following this line of work,

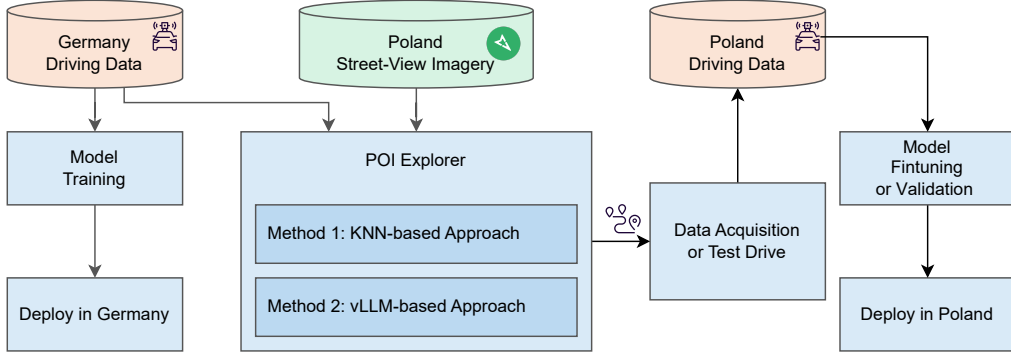


Fig. 2: Workflow of the street-view-guided cross-country data acquisition strategy. In this example, Germany serves as the source country providing training data, while Poland is the target deployment country. Instead of using data from the entire target region, the ADAS model is finetuned or validated using only the selected POIs, enabling more efficient deployment.

we leverage the generalization capability of vLLM for open-vocabulary traffic sign detection and attribute-based cross-country comparison, enabling a more interpretable understanding of domain-level differences.

### III. PROBLEM STATEMENT

In this section, we formally introduce the problem of cross-country POI exploration. We first define the task and its objectives, then describe how to enable controlled and repeatable evaluation through a *collect-detect* protocol. Finally, we provide a mathematical formulation of the problem.

#### A. Problem Protocol

Figure 2 illustrates the workflow of our cross-country POI-exploration protocol. A model is first trained in a source country (e.g., Germany), and the goal is to deploy it in a target country (e.g., Poland). Rather than entering the target region without prior knowledge, our strategy leverages publicly available street-view imagery from platforms such as Google Maps and Mapillary to identify locations that exhibit visual or semantic discrepancies relative to the source-domain data. Locations flagged as POIs, those likely to be unfamiliar or challenging for the model, are added to a prioritized test route. Test engineers can then perform targeted data collection or function validation during a subsequent test drive in the target country. This protocol provides actionable *a priori* insights and reduces unnecessary on-road exploration by focusing attention on locations that matter for cross-country adaptation.

In principle, a more faithful evaluation paradigm for this task is a *detect-collect* protocol: first exploring the target country’s street-view imagery to detect POIs, and performing real-world driving to these locations for data collection or validation. Then we finetune the model on the selected data. A larger performance improvement indicates that more discrepant data are selected. However, executing such a protocol is logically infeasible in research settings, as it would require repeated international test drives for every experiment, resulting in prohibitive cost and time.

To enable systematic evaluation, we adopt a *collect-detect* protocol as a practical and scalable proxy. We start from a pre-collected multi-country driving dataset and retrieve street-view images at the same GPS coordinates of each image in the driving dataset. POI-exploration methods operate on the street-view set and select the top- $k$  discrepant places. The co-located driving data is selected for finetuning the model.

It is important to note that *collect-detect* is not intended to perfectly replicate *detect-collect*. Instead, it provides a controlled, repeatable, and fair environment for comparing different POI-exploration strategies under identical data budgets. The goal is to study the *relative* effectiveness of selection methods, rather than to simulate full-scale deployment behavior.

#### B. Problem Formulation

We formulate the previous introduced problem mathematically. Let  $D_{\text{train}}^S$  denote the source-domain training set, and  $D_{\text{train}}^T$  and  $D_{\text{val}}^T$  the training and validation sets from the target domain. The goal of POI exploration is to select a subset  $D_{\text{train}}^{T,k} \subseteq D_{\text{train}}^T$  of size  $k$  such that finetuning on this subset maximizes target-domain performance. Let  $\mathcal{M}$  be a model pretrained on  $D_{\text{train}}^S$  and  $\mathcal{M}(D_{\text{train}}^{T,k})$  the model after finetuning on the selected subset. With  $\mathcal{P}(\cdot, D_{\text{val}}^T)$  denoting an evaluation function, the data-selection objective is:

$$D_{\text{train}}^{T,k*} = \arg \max_{D_{\text{train}}^{T,k} \subseteq D_{\text{train}}^T} \mathcal{P}(\mathcal{M}(D_{\text{train}}^{T,k}), D_{\text{val}}^T).$$

Since driving data from the target domain is typically unavailable prior to collection, we assume access only to a set of street-view images  $I_T$ , grouped by GPS location. Each location  $\ell$  is associated with a set of retrieved street-view images  $I(\ell) \subseteq I_T$ . A POI-exploration method computes an image-level discrepancy score for each  $x \in I(\ell)$ , and aggregates them into a location-level score  $s(\ell)$ . The top- $k$  locations are then selected:

$$L_T^k = \text{TopK}_\ell(s(\ell)).$$

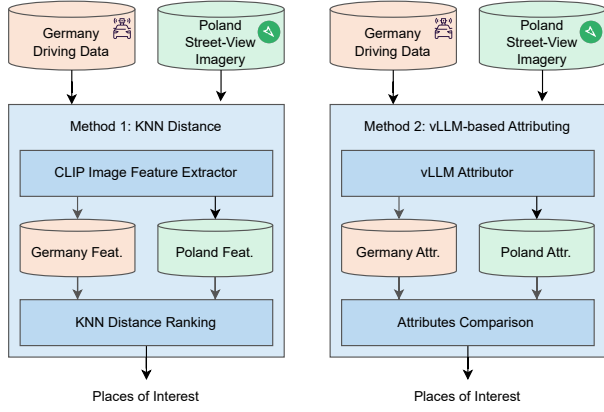


Fig. 3: Two proposed foundation model-based methods to detect POI.

The corresponding driving data at these locations form the fine-tuning subset:

$$D_{\text{train}}^{T,k} = \Phi(L_T^k),$$

where  $\Phi$  maps selected locations to their associated driving logs. Thus, POI exploration reduces to designing a scoring function  $s : \ell \rightarrow \mathbb{R}$  whose induced selection  $D_{\text{train}}^{T,k}$  yields maximal downstream performance in the target domain.

#### IV. METHODOLOGY

In the following two sections, we introduce our proposed two discrepancy scoring methods: KNN-based feature distance and vLLM-based visual attributing. As shown in Figure 3, both methods first extract features / attributes on the source driving data and target street-view data. Then, using a features / attributes distance to calculate the score.

##### A. Method 1: KNN-based Feature Distance Scoring

As discussed in Section II-B, our problem does not follow a standard active-learning setting. To quantify cross-domain differences, we adopt a KNN-based feature distance scoring method inspired by [8]. Instead of the image encoder of the ADAS perception model, we extract a representation  $\mathbf{f}(x)$  using a pretrained foundation vision encoder. Source-domain features are obtained from driving images, whereas target-domain features come from street-view imagery. Given the substantial variability in street-view data (e.g., viewpoints, lighting, and capture devices), a foundation model provides more stable and domain-agnostic representations than the task-specific encoder.

Let  $\mathcal{F}_S = \{\mathbf{f}(x_i^S)\}$  denote the feature set of source-domain images. For a target location (driving log)  $l$ , multiple street-view images may be retrieved. We compute a per-image discrepancy score based on the  $k$ -th nearest neighbor distance to the source-domain feature vectors:

$$s(x) = d_k(\mathbf{f}(x), \mathcal{F}_S),$$

You are given an image. Detect all traffic signs and return structured JSON data.

For each traffic sign, include:  
- a descriptive name (free text)  
- structured attributes  
- high-level category (from a fixed set)

Use the format:  
[  
{  
 "name": "<short\_name\_with\_underscore>",  
 "category": "<one of: regulatory, warning, informational, guide, construction, school\_zone, other>",  
 "attributes": {  
 "shape": "<one of: circle, triangle, rectangle, square, octagon, diamond, inverted\_triangle>",  
 "color": {  
 "border": "<one of: red, white, yellow, black, blue, green, none>",  
 "background": "<one of: red, white, yellow, black, blue, green, none>",  
 "symbol": "<one of: red, white, yellow, black, blue, green, none>"  
 }  
 },  
 "symbol": "<one of: arrow, pedestrian, car, bicycle, stop\_hand, number, none, other>",  
 "text": "<extracted text or 'none'>",  
 "language": "e.g., English, German, Chinese, etc."  
}  
]  
  
Rules:  
- Only return actual traffic signs  
- If the sign has no text, use "text": "none"  
- If the sign uses only symbols (no text), set "language": "none"  
- If no signs are detected, return []  
- Do not return signs on road

Fig. 4: Prompt used for traffic sign attribute extraction.

where  $d_k$  is the  $k$ -th smallest Euclidean distance in the normalized feature space.

To obtain a location-level score  $s(l)$ , we aggregate scores across all images associated with the same driving location. We take the minimum discrepancy to mitigate viewpoint variability:

$$s(l) = \begin{cases} \min_{x \in I(l)} s(x), & \text{if } I(l) \neq \emptyset, \\ 0, & \text{if no street-view image is available,} \end{cases}$$

where  $I(l)$  is the set of retrieved images for location  $l$ . Locations without image returns are assigned a score of zero.

##### B. Method 2: vLLM-based Attribute-Level Scoring

While the KNN-based method captures global visual deviations, our second scoring strategy focuses on fine-grained, traffic-sign-specific semantics. Instead of comparing image-level embeddings, we rely on a vLLM to extract structured traffic-sign attributes from street-view imagery, enabling more interpretable and controllable POI identification.

*Attribute extraction.:* As shown in Figure 4, each street-view image is processed with a structured prompt to detect all visible traffic signs and annotate them using a predefined attribute ontology. Each detected sign is represented as an attribute vector

$$\mathbf{a} = (a_{\text{category}}, a_{\text{shape}}, a_{\text{color.border}}, a_{\text{color.background}}, \\ a_{\text{color.symbol}}, a_{\text{symbol}}, a_{\text{text}}, a_{\text{language}}),$$

where each  $a$  corresponds to one traffic-sign attribute. A driving location  $l$  may have multiple retrieved images, and each image may contain multiple signs. We aggregate all

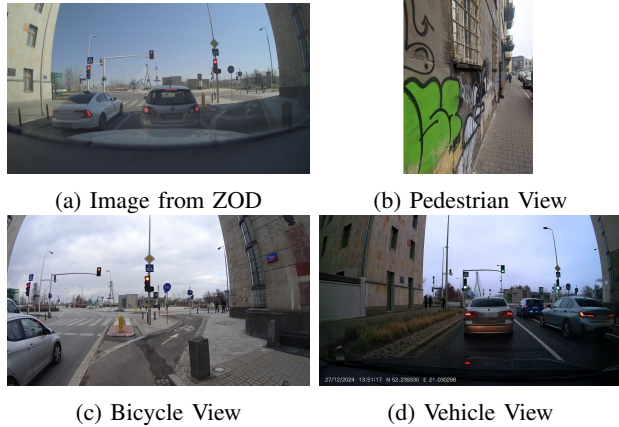


Fig. 5: Examples of co-located images. (a) shows the on-board image from the ZOD [2] dataset, while (b)-(d) are street-view images within a 10 m radius from Mapillary [4].

detected signs for location  $l$  and remove duplicates, yielding a unique sign-attribute set

$$A(l) = \{\mathbf{a}_1, \mathbf{a}_2, \dots, \mathbf{a}_M\}.$$

To calculate the discrepancy score from attributes, we first construct the set of all unique sign attribute vectors based on the driving data of the source country:

$$A_S = \{\mathbf{a}_i^S\}.$$

For a target-domain sign  $\mathbf{a} \in A(l)$ , we measure its semantic deviation from the source by comparing it to the most similar source sign in  $A_S$  using a Hamming distance over attributes:

$$d(\mathbf{a}, \mathbf{a}') = \sum_{j=1}^K \mathbf{1}[a_j \neq a'_j],$$

where  $K$  is the total number of attributes to describe a traffic sign ( $K = 8$  in our setup), and

$$d(\mathbf{a}, A_S) = \min_{\mathbf{a}' \in A_S} d(\mathbf{a}, \mathbf{a}').$$

The location-level discrepancy score is then defined as the sum of per-sign deviations:

$$s(l) = \sum_{\mathbf{a} \in A(l)} d(\mathbf{a}, A_S).$$

A higher score indicates that the location contains more traffic signs whose attributes differ from those observed in the source domain (e.g., new shapes, color schemes, symbols, or languages). Such locations are prioritized as discrepant POI.

## V. EXPERIMENTAL SETUP

### A. Dataset Preparation

Following the *collect–detect* protocol introduced in Section III-A, we use the ZOD dataset [2] as the driving-data source. ZOD provides multi-country driving logs with high-precision GPS coordinates and traffic-sign annotations. We

focus on the four countries with the largest data volume: Germany (DE), Poland (PL), Sweden (SE), and France (FR). Germany serves as the source domain for pretraining, while the other three serve as target domains. Each country-specific subset is split into training and validation sets using a 9:1 ratio.

Street-view imagery is obtained using the Mapillary API [4], which supports GPS-based retrieval. For each driving-log coordinate in the training split, we request all available street-view images within a 10 m radius. The number of returned images varies across locations (from zero to multiple). Up to 10 images are retained per location, ranked by proximity to the query coordinate. The final retrieval statistics are summarized in Table I: overall, more than 80% of driving-log locations successfully return at least one street-view image. For locations where no street-view imagery is available, we assign a default POI score of zero. Figure 5 illustrates typical retrieved samples, where the images originate from different viewpoints and capture devices, highlighting the challenges posed by street-view data.

### B. Model Under Test

We choose TSD as the ADAS perception model to do cross-country deployment for three reasons: (1) TSD is essential for traffic-rule interpretation, (2) detection performance is highly sensitive to country-specific regulatory differences, and (3) high-quality annotations are already provided in ZOD.

We adopt RetinaNet [11] implemented in Detectron2 [31], owing to its favorable accuracy-efficiency trade-off for on-board deployment. The model is first pretrained on the Germany training set for 20 epochs with  $batch\_size = 8$  using the Adam optimizer with a learning rate of 0.0025. For adaptation, the model is finetuned using  $k$  samples from the target-domain training set, where the selected  $k$ -subset is determined by a POI exploration method.

Performance is evaluated using Average Precision (AP) at an IoU threshold of 0.5. Higher AP improvements after finetuning indicate that the selected subset is more informative. We evaluate multiple data budgets, expressed as percentages of the target-domain training set. Let  $\alpha \in \{5\%, 10\%, 15\%, 20\%, 25\%, 50\%, 75\%\}$  denote the sampling ratio. For each  $\alpha$ , the actual subset size is  $k = \alpha \cdot |D_{\text{train}}^T|$ , and we finetune the pretrained model on  $D_{\text{train}}^{T,k}$ . Each finetuning run spans 10 epochs with the same hyperparameters as pretraining.

### C. POI-Exploration Method Details

We compare three POI exploration methods:

- a) *Random Selection (Baseline)*.: A uniform random subset of size  $k$  is selected without using street-view imagery.
- b) *KNN-based method*.: We use the ViT-L/14 image encoder from CLIP [22] as the image encoder due to its strong generalization ability. For KNN algorithm, we select  $k = 10$ , following one setup from the original paper [8]
- c) *vLLM-based method*.: We employ gpt-5-mini (model version 2025-08-07) from OpenAI [7] conduct visual attributing. While single-image API calls require approximately 5 s per image, we leverage batch-mode processing

TABLE I: Statistics of the ZOD and street-view image retrieval results from Mapillary. Over 80% of logs yielding at least one image. Only data from Poland (PL), Germany (DE), Sweden (SE), and France (FR) are considered, as the remaining countries in ZOD do not contain sufficient samples for country-specific training.

Country	Logs in ZOD	Logs w. Traffic Sign	Has Street-View Image Return	Ratio of Logs with Mapillary Returns
PL	30,483	23,207	20,022	86.28%
DE	24,816	19,492	17,094	87.70%
SE	17,647	8,280	6,912	83.48%
FR	11,785	7,666	6,560	85.57%

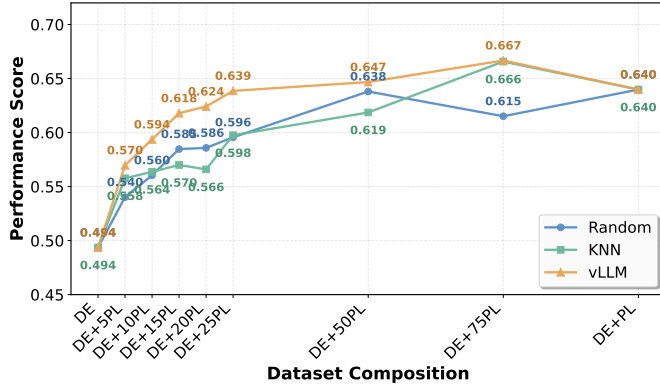


Fig. 6: The TSD model is pretrained on ZOD Germany dataset and then finetuned with different portion of ZOD (Poland) dataset (5%, 10%, 15%, 20%, 25%, 50%, 75%, 100%). Three POI exploration methods are compared: Random Selection, KNN-based method, vLLM-based method.

(up to 50k images per batch), which significantly accelerates scoring and enables large-scale evaluation.

## VI. EVALUATION

We evaluate the effectiveness of the street-view-guided data acquisition strategy and the proposed POI scoring methods. Three research questions (RQ) are answered in the following sections:

- RQ1: Can proposed methods achieve comparable performance with requiring *less* target-domain data, or equivalently, do they achieve *greater* performance improvement under the same data budget?
- RQ2: Can the strategy generalize across different target countries, demonstrating consistent benefits beyond a single deployment scenario?
- RQ3: Do the selected POIs reflect meaningful cross-country differences that can be qualitatively interpreted from street-view imagery?

### A. RQ1: Finetuning with Different Portions of Target Data

We first report the finetuning performance when varying the amount of Polish training data added on top of the German pretrained model. Several observations emerge.

As shown in Figure 6, finetuning with only a small portion of PL data already yields significant performance gains. For example, using 10–25% of the target-domain data results in AP

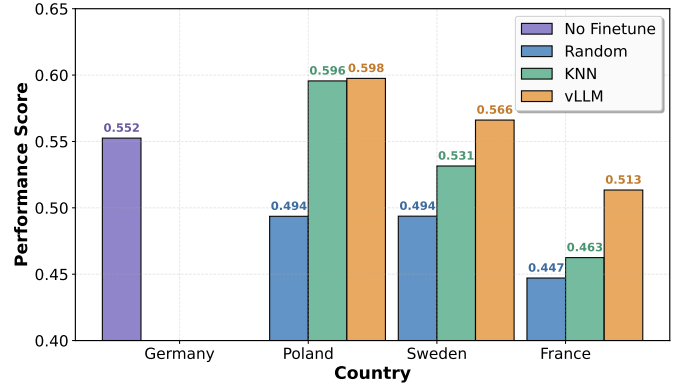


Fig. 7: The TSD model is pretrained on ZOD (Germany) dataset, and then finetuned with 25% of ZOD (Poland, Sweden, France) dataset.

values of 0.594–0.639 with the vLLM-based scoring method, approaching the performance of full-data finetuning (0.640). This confirms that exhaustive target-domain data collection is not strictly necessary: a carefully selected subset can recover most of the achievable adaptation benefit.

Second, the proposed vLLM-based scoring consistently outperforms both random sampling and the KNN-based method across nearly all data budgets. With only 25% of the target-domain data, the vLLM approach already surpasses the performance achieved by using 50% of the data under random selection. The improvement is particularly pronounced at low data budgets (5–25%), where selecting semantically distinctive locations is critical.

In contrast, the KNN-based method provides only a marginal average improvement over random sampling (+0.03 AP) and exhibits high variance across runs. This instability arises because CLIP embeddings capture global scene semantics rather than traffic-sign-specific cues, making the feature-distance measure sensitive to irrelevant visual variations in street-view imagery.

Finally, we observe that selectively chosen data can even surpass full-data training. At 75% of the PL data, vLLM and KNN achieve an AP of 0.667/0.666, exceeding the full-data finetuning 0.640. According to [32], this can be explained by the presence of redundancy and noise in the full dataset, and further emphasizes that the goal of POI exploration is not to gather more data, but to gather *better* data.

### B. RQ2: Finetuning Across Different Countries

We further evaluate whether the proposed POI exploration strategy generalizes across different target countries. Based on the results in Figure 6, we adopt a 25% data budget for all target domains, as performance largely saturates beyond this point. Starting from the German-pretrained model, we finetune on 25% of the training data from Poland, Sweden, and France and report the corresponding validation performance. For reference, we also include the German validation AP to indicate in-domain performance. The results are shown in Figure 7.

Across all three target countries, the no-finetuning model performs worse than on Germany, confirming the presence of significant cross-country domain shift and the necessity of target-domain data acquisition. Finetuning with 25% of the target data yields clear improvements in all cases, closing much of the performance gap.

Among all data-selection strategies, the proposed vLLM-based method consistently achieves the highest performance in every country. The gains over random selection are substantial: +0.043 AP in Poland, +0.054 in Sweden, and +0.076 in France. KNN-based method also improves over random in Sweden and France but exhibits marginal benefit in Poland (+0.002), showing lower stability across domains. These results demonstrate that vLLM-based visual attribution is more reliable in identifying discrepant POIs that support effective cross-country adaptation.

### C. RQ3: Qualitative Output Analysis and Failure Cases

Figure 8 shows representative examples from the two methods. Subfigures (a)-(d) come from the top-ranked outputs of the vLLM-based method. Examples (a) and (b) illustrate successful identification of country-specific traffic signs in Poland. In (c), the sign detected in the street-view image is not visible in the driving data due to a mismatch of viewpoint. Example (d) shows a temporal discrepancy: the guide sign appears in the street-view image, but had been removed by the time the test vehicle passed the location. Under the adopted *collect-detect* protocol, such spatial and temporal mismatches are expected and do not indicate method failure; instead, they reflect real-world factors that a full *detect-collect* pipeline would naturally address.

Figure (e) shows a typical failure from the KNN-based method. Although with a high discrepancy score, the street-view image does not contain any traffic-scene content. This highlights the limitation of general image embedding for task-specific data acquisition and the advantage of vLLM-based reasoning in focusing on semantically relevant POIs.

### D. Cost Analysis

We estimate the computational cost of performing large-scale street-view analysis using the gpt-5-mini API [33]. Based on our measurements, processing one image requires on average 200 tokens, including both prompt and response. Assuming one street-view image every 20m, the cost of

analyzing a road network of length  $L$  is

$$\text{Cost}(L) = \frac{L}{20 \text{ m}} \times 200 \text{ tokens} \times \frac{\$2}{10^6}.$$

For a 100,000 km network, this yields an estimated cost of roughly \$2,000. Note that this is a coarse, order-of-magnitude approximation; storage, retrieval, bandwidth, and other system-level costs are not included.

TABLE II: Estimated vLLM processing cost for full road network analysis (1 image per 20m, 200 tokens per image, \$2 per million tokens). National road length data from [34].

Country	Road Length (km)	Estimated Cost (USD)
Poland	429,800	\$8,596
France	1,053,215	\$21,064
Sweden	573,134	\$11,463

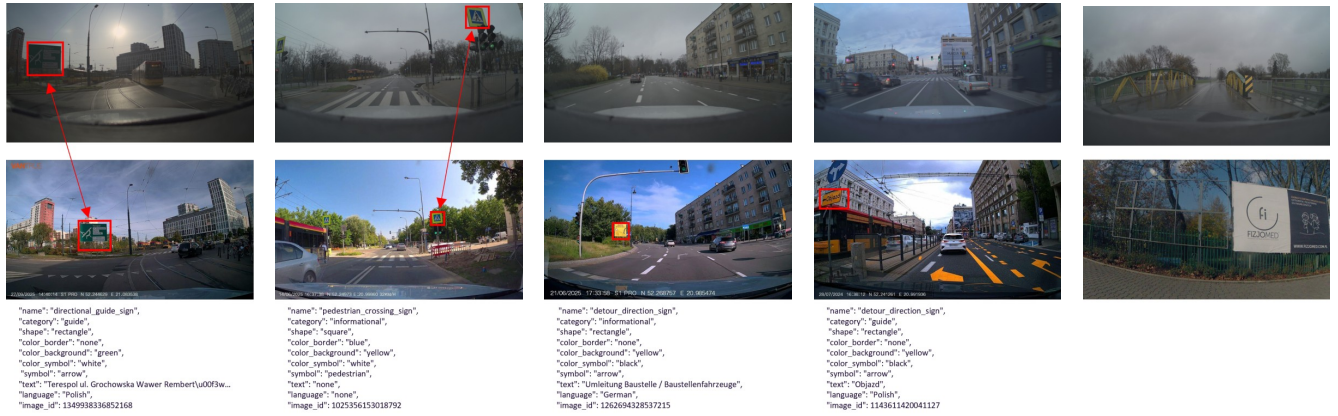
Using publicly compiled national road-length statistics [34], we approximate the vLLM processing cost for Poland, France, and Sweden. Table II reports the estimated cost assuming full-network coverage. In practice, an ADAS deployment analyzes only selected operational regions (e.g., major cities or specific roads), and street-view coverage is incomplete in some areas, so the actual cost is typically far lower than the full-coverage estimate. Although we do not quantify real-world test-drive costs, on-road data collection is generally considered far more expensive and logically demanding than automated street-view analysis. Consequently, a processing cost of a few thousand dollars is typically acceptable in practice.

## VII. CONCLUSION

This paper presented an efficient street-view-guided data acquisition strategy for ADAS deployment. Instead of relying solely on costly large-scale test drives, we leverage publicly available street-view imagery to identify POIs in the target country prior to real-world data collection. We designed a *collect-detect* protocol and built a co-located driving and street-view dataset. The proposed vLLM-based method requires only half of the data to achieve the same level of model improvement. Future work will extend this strategy to additional perception tasks and incorporate richer scene attributes for improved POI discovery.

## REFERENCES

- [1] J. Quiñonero-Candela *et al.*, Eds., *Dataset Shift in Machine Learning*. Cambridge, MA: MIT Press, 2022.
- [2] M. Alibeigi, W. Ljungbergh, A. Tonderski, G. Hess, A. Lilja, C. Lindström, D. Motorniuk, J. Fu, J. Widahl, and C. Petersson, “Zenseact open dataset: A large-scale and diverse multimodal dataset for autonomous driving,” in *Proceedings of the IEEE/CVF International Conference on Computer Vision*, 2023.
- [3] “Google maps,” <https://www.google.com/maps>, accessed: 2025-02-13.
- [4] “Mapillary api documentation,” <https://www.mapillary.com/developer/api-documentation>, accessed: 2025-11-13.
- [5] M. Long, Y. Cao, J. Wang, and M. Jordan, “Learning transferable features with deep adaptation networks,” in *International conference on machine learning*. PMLR, 2015, pp. 97–105.
- [6] A. Yang, A. Li, B. Yang, B. Zhang, B. Hui, B. Zheng, B. Yu, C. Gao, C. Huang, C. Lv *et al.*, “Qwen3 technical report,” *arXiv preprint arXiv:2505.09388*, 2025.



(a) Detected sign      (b) Detected sign      (c) Viewpoint mismatch      (d) Temporary removal      (e) KNN failure

Fig. 8: Qualitative POI retrieval examples in Poland. (a)–(d) Results from the proposed VLLM-based method; (e) KNN baseline. Top: ZOD driving images. Bottom: Mapillary street-view. (a) Correct guide sign. (b) Pedestrian crossing with yellow background. (c) Missing due to viewpoint mismatch. (d) Missing due to temporary removal. (e) High-score KNN false positive.

- [7] J. Achiam, S. Adler, S. Agarwal, L. Ahmad, I. Akkaya, F. L. Aleman, D. Almeida, J. Altenschmidt, S. Altman, S. Anadkat *et al.*, “Gpt-4 technical report,” *arXiv preprint arXiv:2303.08774*, 2023.
- [8] Y. Sun, Y. Ming, X. Zhu, and Y. Li, “Out-of-distribution detection with deep nearest neighbors,” in *International conference on machine learning*. PMLR, 2022, pp. 20 827–20 840.
- [9] J. Redmon, S. Divvala, R. Girshick, and A. Farhadi, “You only look once: Unified, real-time object detection,” in *Proceedings of the IEEE conference on computer vision and pattern recognition*, 2016, pp. 779–788.
- [10] S. Ren, K. He, R. Girshick, and J. Sun, “Faster r-cnn: Towards real-time object detection with region proposal networks,” *IEEE transactions on pattern analysis and machine intelligence*, vol. 39, no. 6, pp. 1137–1149, 2016.
- [11] T.-Y. Lin, P. Goyal, R. Girshick, K. He, and P. Dollár, “Focal loss for dense object detection,” in *Proceedings of the IEEE international conference on computer vision*, 2017, pp. 2980–2988.
- [12] N. Carion, F. Massa, G. Synnaeve, N. Usunier, A. Kirillov, and S. Zagoruyko, “End-to-end object detection with transformers,” in *European conference on computer vision*. Springer, 2020, pp. 213–229.
- [13] P. Ren, Y. Xiao, X. Chang, P.-Y. Huang, Z. Li, B. B. Gupta, X. Chen, and X. Wang, “A survey of deep active learning,” *ACM computing surveys (CSUR)*, vol. 54, no. 9, pp. 1–40, 2021.
- [14] W. H. Beluch, T. Genewein, A. Nürnberg, and J. M. Köhler, “The power of ensembles for active learning in image classification,” in *Proceedings of the IEEE conference on computer vision and pattern recognition*, 2018, pp. 9368–9377.
- [15] Y. Gal, R. Islam, and Z. Ghahramani, “Deep bayesian active learning with image data,” in *International conference on machine learning*. PMLR, 2017, pp. 1183–1192.
- [16] Y. Ganin, E. Ustinova, H. Ajakan, P. Germain, H. Larochelle, F. Laviolette, M. March, and V. Lempitsky, “Domain-adversarial training of neural networks,” *Journal of machine learning research*, vol. 17, no. 59, pp. 1–35, 2016.
- [17] M. Ghifary, W. B. Kleijn, M. Zhang, D. Balduzzi, and W. Li, “Deep reconstruction-classification networks for unsupervised domain adaptation,” in *European conference on computer vision*. Springer, 2016, pp. 597–613.
- [18] J. Liang, D. Hu, and J. Feng, “Do we really need to access the source data? source hypothesis transfer for unsupervised domain adaptation,” in *International conference on machine learning*. PMLR, 2020, pp. 6028–6039.
- [19] C. Guo, G. Pleiss, Y. Sun, and K. Q. Weinberger, “On calibration of modern neural networks,” in *International conference on machine learning*. PMLR, 2017, pp. 1321–1330.
- [20] S. Garg, S. Balakrishnan, Z. C. Lipton, B. Neyshabur, and H. Sedghi, “Leveraging unlabeled data to predict out-of-distribution performance,” *arXiv preprint arXiv:2201.04234*, 2022.
- [21] Y. Wu, D. Slieter, A. Abouelazm, C. Hubschneider, and J. M. Zöllner, “Laneperf: a performance estimation framework for lane detection,” *arXiv preprint arXiv:2507.12894*, 2025.
- [22] A. Radford, J. W. Kim, C. Hallacy, A. Ramesh, G. Goh, S. Agarwal, G. Sastry, A. Askell, P. Mishkin, J. Clark *et al.*, “Learning transferable visual models from natural language supervision,” in *International conference on machine learning*. PMLR, 2021, pp. 8748–8763.
- [23] D. Jiang, J. Lin, X. Zhang, X. Yang, Z. Li, and W. X. Zhao, “From clip to dino: Visual encoders shout in multi-modal large language models,” *arXiv preprint arXiv:2310.08825*, 2023.
- [24] Y. Wu, D. Slieter, V. Subramanian, A. Abouelazm, R. Bohn, and J. M. Zöllner, “Why braking? scenario extraction and reasoning utilizing llm,” *arXiv preprint arXiv:2507.15874*, 2025.
- [25] Y. Zhao, W. Xiao, T. Mihalj, J. Hu, and A. Eichberger, “Chat2scenario: Scenario extraction from dataset through utilization of large language model,” in *2024 IEEE Intelligent Vehicles Symposium (IV)*. IEEE, 2024, pp. 559–566.
- [26] C. Sima, K. Renz, K. Chitta, L. Chen, H. Zhang, C. Xie, J. Beißwenger, P. Luo, A. Geiger, and H. Li, “Drivelm: Driving with graph visual question answering,” in *European conference on computer vision*. Springer, 2024, pp. 256–274.
- [27] X. Tian, J. Gu, B. Li, Y. Liu, Y. Wang, Z. Zhao, K. Zhan, P. Jia, X. Lang, and H. Zhao, “Drivevlm: The convergence of autonomous driving and large vision-language models,” *arXiv preprint arXiv:2402.12289*, 2024.
- [28] L. Zhong, F. Rosenthal, J. Sicking, F. Hüger, T. Bagdonat, H. Gottschalk, and L. Schwinn, “Focus: Internal milm representations for efficient fine-grained visual question answering,” *arXiv preprint arXiv:2506.21710*, 2025.
- [29] K. Chen, X. Jiang, Y. Hu, X. Tang, Y. Gao, J. Chen, and W. Xie, “Ovarnet: Towards open-vocabulary object attribute recognition,” in *Proceedings of the IEEE/CVF conference on computer vision and pattern recognition*, 2023, pp. 23 518–23 527.
- [30] M. Chen, C. Zhao, and Q. Xu, “Hibug2: Efficient and interpretable error slice discovery for comprehensive model debugging,” *arXiv preprint arXiv:2501.16751*, 2025.
- [31] Y. Wu, A. Kirillov, F. Massa, W.-Y. Lo, and R. Girshick, “Detectron2,” <https://github.com/facebookresearch/detectron2>, 2019.
- [32] M. Paul, S. Ganguli, and G. K. Dziugaite, “Deep learning on a data diet: Finding important examples early in training,” *Advances in neural information processing systems*, 2021.
- [33] OpenAI, “Api pricing,” <https://openai.com/api/pricing/>, 2025, accessed: 2025-11-14.
- [34] Wikipedia contributors, “List of countries by road network size,” [https://en.wikipedia.org/wiki/List\\_of\\_countries\\_by\\_road\\_network\\_size](https://en.wikipedia.org/wiki/List_of_countries_by_road_network_size), 2025, accessed: 2025-11-14.